Seasonal circulations in the Malay Peninsula Eastern continental shelf from a wave–tide–circulation coupled model

Fredolin T. Tangang · Changsui Xia · Fangli Qiao · Liew Juneng · Feng Shan

Abstract A wave–tide–circulation coupled model based on Princeton Ocean Model is established to study the seasonal circulation in the Malay Peninsula Eastern Continental Shelf region. The model successfully reconstructs the observed seasonal variation of the circulation in the region, as well as the main currents. The simulated tidal harmonic constants, sea surface temperature, and sea surface height anomaly agree with the observations well. The model results show that the upper-layer circulation in the region is mainly controlled by the monsoon winds, while there are two transitions in spring and fall. An anti-cyclonic eddy is present off the Peninsular Malaysia's east coast in summer, centered at 5°N and 105.5°E, both in the TOPEX/Poseidon data and in the model. Numerical experiments show that the wind stress curl and bathymetry steering are responsible for its formation.

Keywords Malay Peninsula Eastern continental shelf · Seasonal circulation · Wave–tide–circulation coupled model

F. T. Tangang · L. Juneng
Climate and Ocean Analysis Laboratory, Research Centre for Tropical Climate Change System (IKLIM), Faculty of Science and Technology, Universiti Kebangsaan Malaysia, Bangi, Selangor, Malaysia

C. Xia (✉) · F. Qiao · F. Shan
First Institute of Oceanography, State Oceanic Administration (SOA), Qingdao, China
e-mail: xiacs@fio.org.cn

1 Introduction

The Malay Peninsula Eastern Continental Shelf (MPECS) is situated in the southern part of the South China Sea (SCS). The SCS is the largest marginal sea in the Southeast Asia (Fig. 1). The maximum depth of the SCS is more than 5,000 m in the middle of the basin, but it is much shallower towards the southern part, especially in the Sunda Shelf region and in the Gulf of Thailand where depth is less than 100 m. The SCS is connected to the western Pacific Ocean through the Taiwan Strait and Luzon Strait; much of the water mass and heat exchanges with the Pacific Ocean are through the Luzon Strait. The SCS is also connected to the Sulu Sea through the Mindoro Strait and Balabac Channel, and at its southern end, to the Java Sea through the Gasper and Karimata Straits and to the Indian Ocean through the Strait of Malacca.

The circulation in the SCS is basically monsoon driven. Strong monsoon winds during winter (DJF) result in high wind stress of over 0.1 Nm^{-2} especially over the central SCS. However, over the southern part, especially over the Sunda Shelf area and the Gulf of Thailand, the wind stress is less than 0.1 Nm^{-2} in winter (Fig. 2). The summer winds (JJA) are relatively weaker, less than 0.1 Nm^{-2}. The winds during autumn (SON) and spring (MAM) are even weaker.

The circulation pattern in the SCS has been the subject of many investigations since the earlier publications of the schematic surface current charts based on the observed drift current data by Dale (1956) and the study by Wyrtki (1961). Since the 1990s, remote sensing satellite data have been used widely to study the surface circulation in the SCS (e.g., Li et al. 2000; Wang et al. 2001). Fang et al. (2002) studied the seasonal circulation patterns of the upper layer in the southern SCS using the CTD and ADCP data. The in situ data show that in summer the upper layer circulation of the southern SCS is dominated by an anti-cyclonic gyre, while
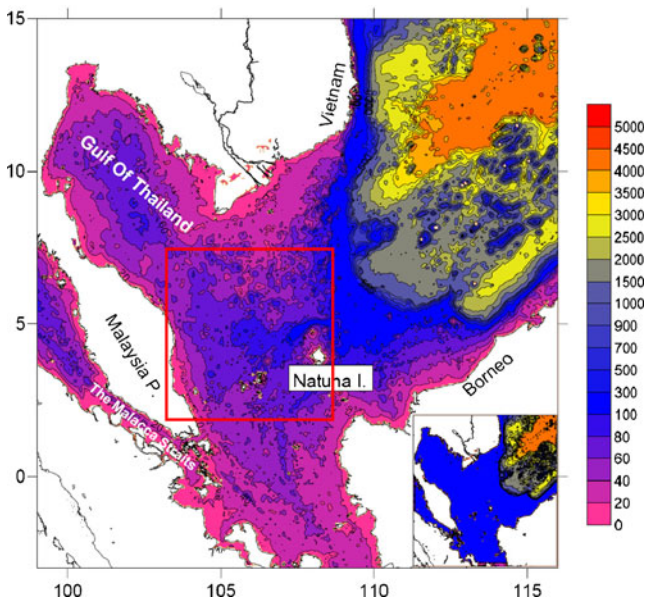
Fig. 1 Model domain and bathymetry, the small figure shows the bathymetry in the experiment with flat bottom in the region shallower than 100 m (unit: m)
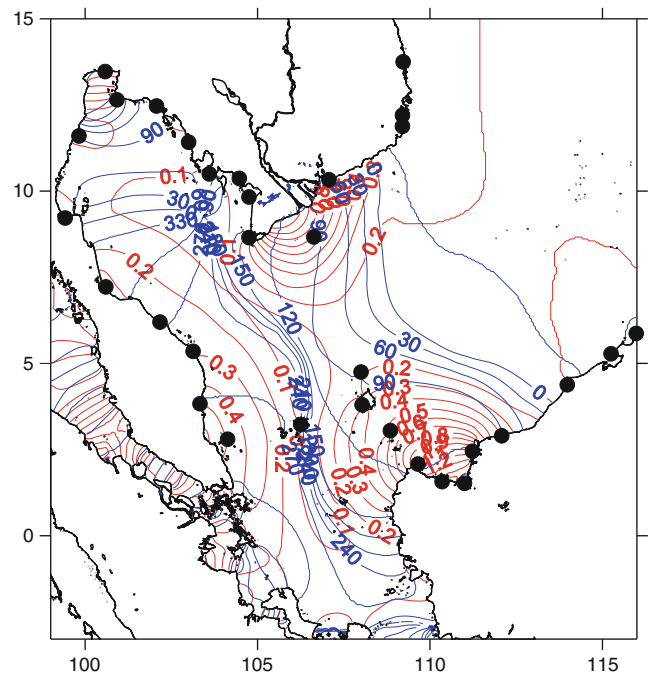

Fig. 3 M_2 co-tidal chart simulated using the model with homogeneous water. Blue and Red lines show the distributions of phase lag (in degrees and referred to the Beijing standard time (UT + 8 hours)) and amplitude (in meters). Black dots are the locations of the tidal observation stations
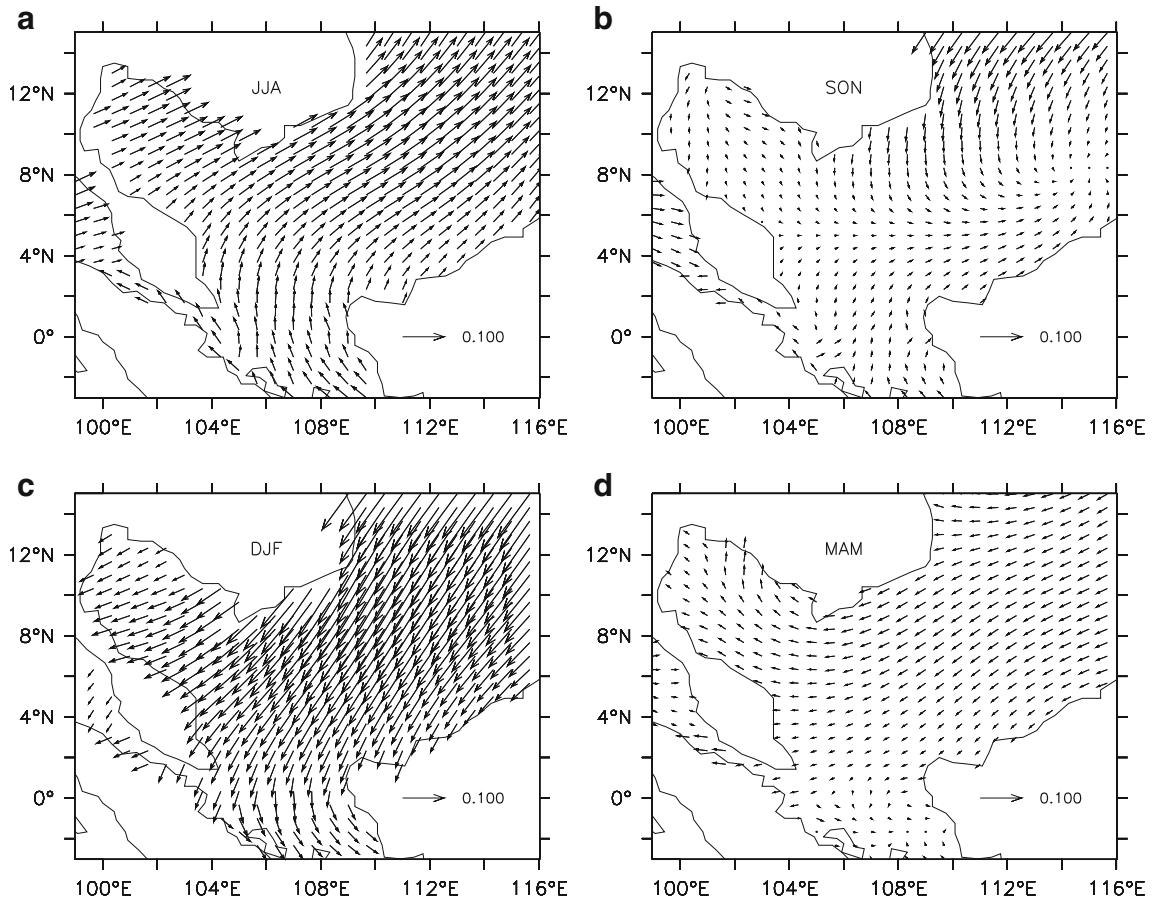

Fig. 2 Wind stress forcing fields for JJA, SON, DJF, and MAM from COADS wind dataset (units: N/m^2)
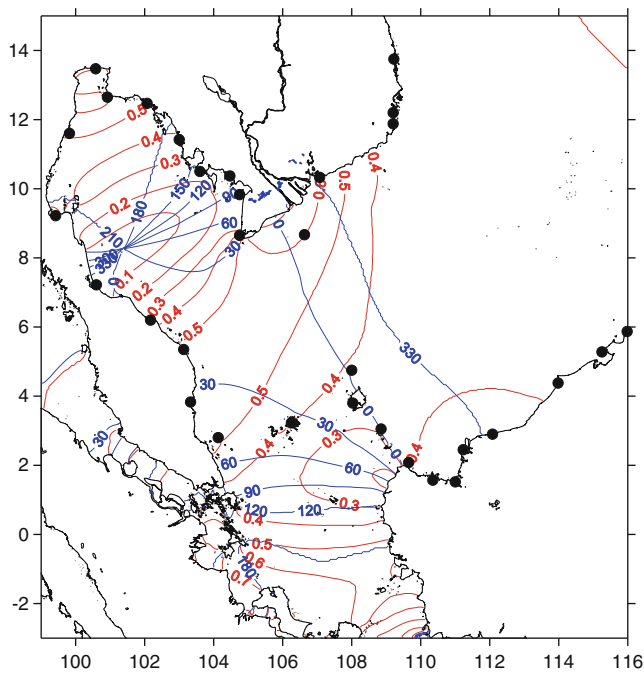
Fig. 4 Same as Fig. 3, except for K_1

in winter a stronger cyclonic gyre exists in the west part of the southern SCS and a weaker anti-cyclonic circulation in the east part of the SCS. Their study area is to the east of 106°E and north of 3°N, and does not cover the major part of the MPECS. Fang et al. (2010) studied the volume, heat, and freshwater transports from the SCS to the Indonesian Seas in the boreal winter of 2007–2008 based on Acoustic-Doppler-current-profiler observations. The observations showed a mean volume transport of 3.6 Sv through the Karimata Strait (including the Gaspar Strait) from the SCS to the Indonesian Seas from January 13 to February 12, 2008.

There have also been a number of numerical studies on the SCS circulation (e.g., Shaw and Chao 1994; Chu et al. 1999; Yang et al. 2002). Chu et al. (1999) studied the seasonal circulation of the SCS using the Princeton Ocean Model (POM) with a 20-km-horizontal resolution and 23 sigma layers. The simulated SCS surface circulation is generally anti-cyclonic (cyclonic) during the summer (winter) monsoon with strong west boundary current. Yang et al. (2002) studied the SCS circulation, also using the POM. Their results show that most of the seasonal

Fig. 5 a Comparison between the observed and modeled constants of the M_2 tide. Left: amplitude; Right: phase. Station locations are shown with black dots in Fig. 3. The observed tidal harmonic constants are from British Admiralty Tide and Tidal Stream Tables. **b** Same as Fig. 5a, except for K_1
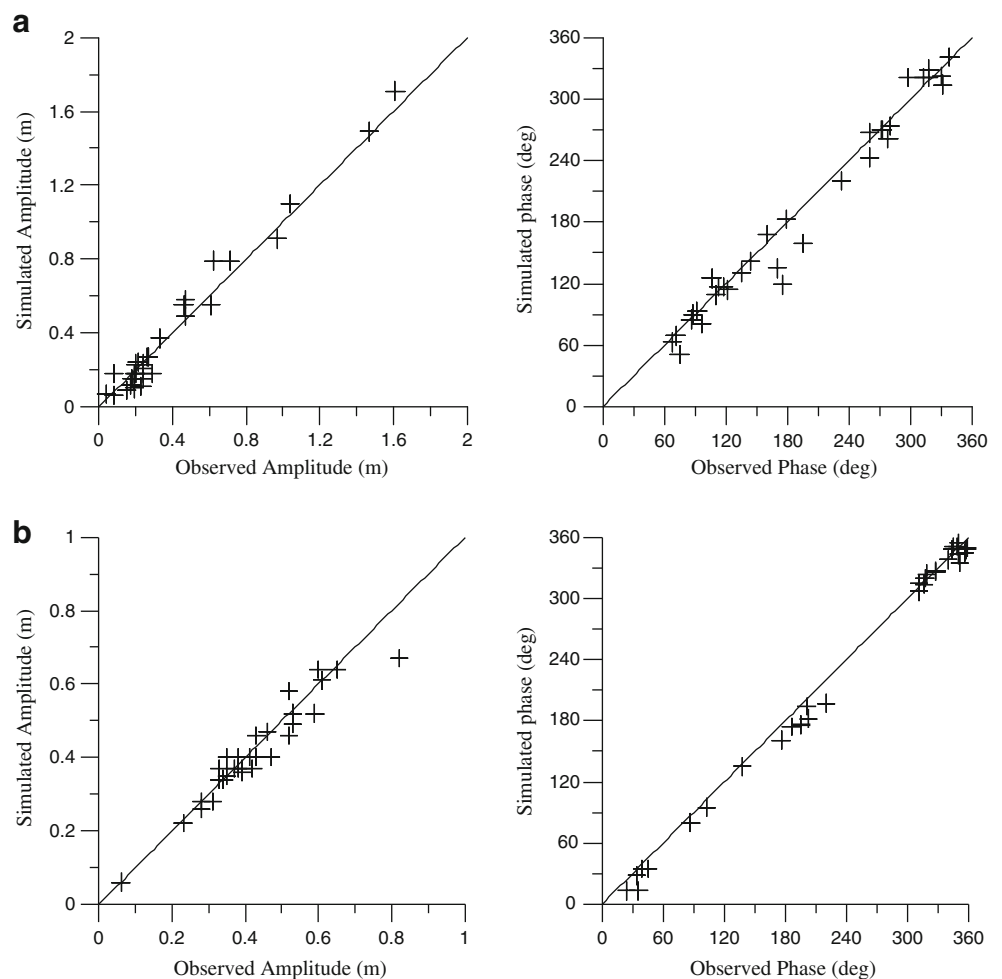
variability in the SCS is controlled predominantly by wind forcing. With regards to tide modeling, Fang et al. (1998) simulated the principal tidal constituents M_2, S_2, K_1, and O_1 in the SCS, Gulf of Tonkin, and Gulf of Thailand, and investigated the energy budgets in these areas. Zu et al. (2008) studied the tides and their dynamic processes in the SCS by assimilating TOPEX/Poseidon altimetry data into a barotropic tide model for the eight major constituents (M_2, S_2, K_1, O_1, N_2, K_2, P_1, and Q_1) using a tidal data inversion scheme.

Fang et al. (1998) provided a comprehensive survey of the studies on the SCS upper-ocean circulation. Based on the previous studies, they concluded that the circulation in the northern SCS is jointly driven by monsoon winds and the Kuroshio intrusion through the Luzon Strait. The most prominent features of the circulation in the northern SCS are the northwest Luzon cyclonic gyre, the northwest Luzon cyclonic eddy, the Northwest Luzon Coastal Current, and the Guangdong Coastal Current. On the other

hand, the circulation in the southern SCS is mainly controlled by the monsoon winds. The main circulation features are the SCS Southern Cyclonic Gyre during winter and the SCS anti-cyclonic gyre during summer. However, the circulation in the central SCS is governed by monsoon winds and the interaction between circulations in the southern SCS and northern SCS. Hu et al. (2000) also provided a comprehensive review of the progress on the SCS upper-ocean circulation.

Most of these previous studies focus on the whole SCS, the southern SCS, or northern SCS. The circulation pattern of the MPECS is much less studied. The MPECS and the Strait of Malacca are important routes for international shipping. This study will focus on the circulation structure and dynamic mechanism in the MPECS region. The rest of the paper is organized as follows. The wave–tide–circulation coupled model and experiment design are described in Section 2. The simulated tidal harmonic constants of M_2 and K_1 are discussed in Section 3, the validation of the
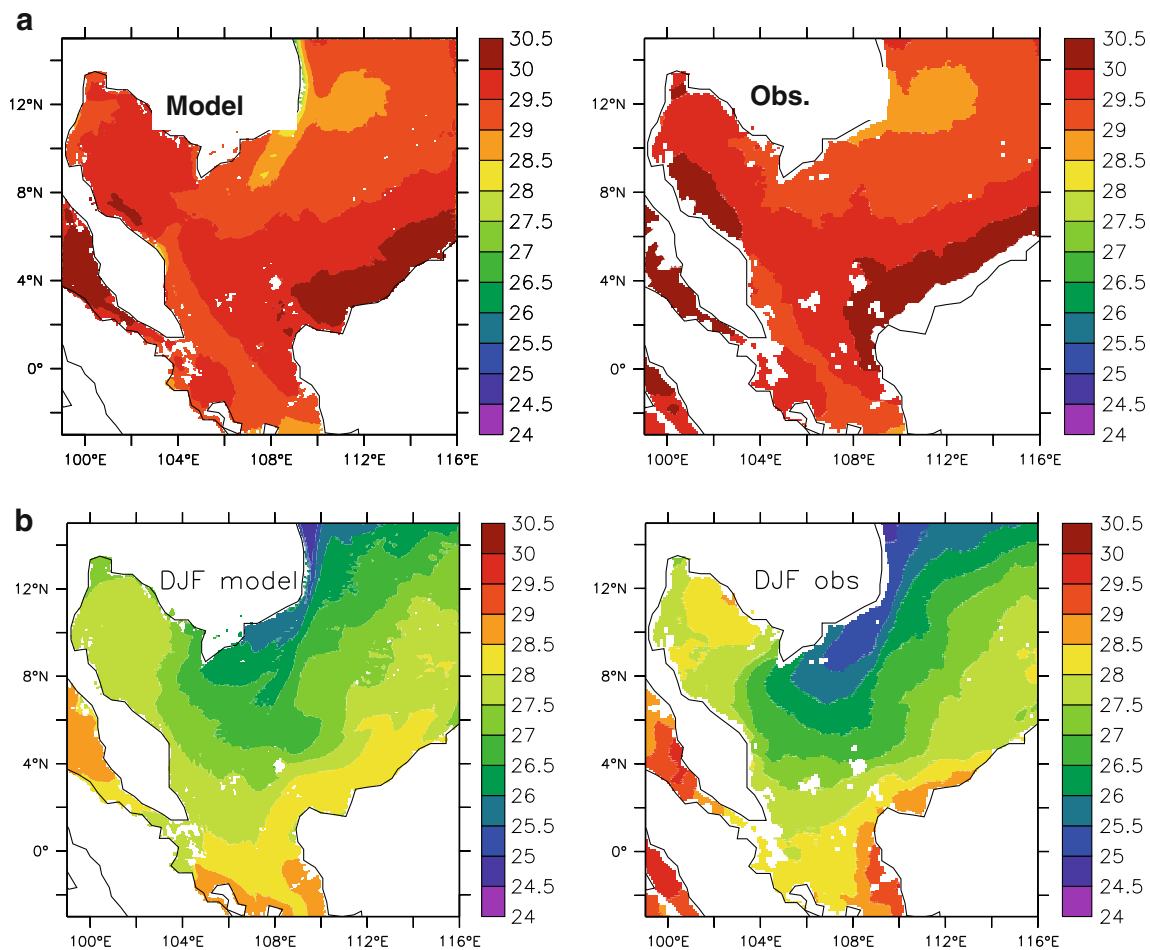

Fig. 6 a Modeled (left) and observed (right, Reynolds and Smith) surface temperature in summer (JJA). b Modeled (left) and observed (right, Reynolds and Smith) surface temperature in winter (DJF)

simulated sea surface temperature and sea surface height is also given in Section 3. The simulated circulation results and dynamic mechanism are analyzed in Section 4, with a focus on the anti-cyclonic gyre off the Peninsular Malaysia's coast centered at 5°N and 105.5°E in summer. Finally, conclusions are given in Section 5.

2 Numerical ocean model

2.1 Model description

The numerical model used in this study is the wave–tide–circulation coupled model, developed by the Laboratory of Marine Sciences and Numerical Modeling (MASNUM),

State Oceanic Administration of China. The circulation component of the coupled model is based on the POM, which uses the level 2.5 Mellor and Yamada (M-Y) turbulence closure scheme (Mellor and Yamada 1982) to calculate vertical turbulence mixing. In this setup, the vertical viscosity and diffusivity are set to a combination function of turbulence mixing length, turbulence kinetic energy, and the Richardson number. However, a number of studies indicated that such a scheme has its shortcoming by overestimating sea surface temperature (SST) and producing too shallow upper mixed layer due to the underestimate of surface mixing and mixed layer depth. Using the MASNUM wave number spectral model, the wave-induced mixing term Bv is added to the vertical viscosity and diffusivity in the M-Y scheme. The study by Qiao et al.
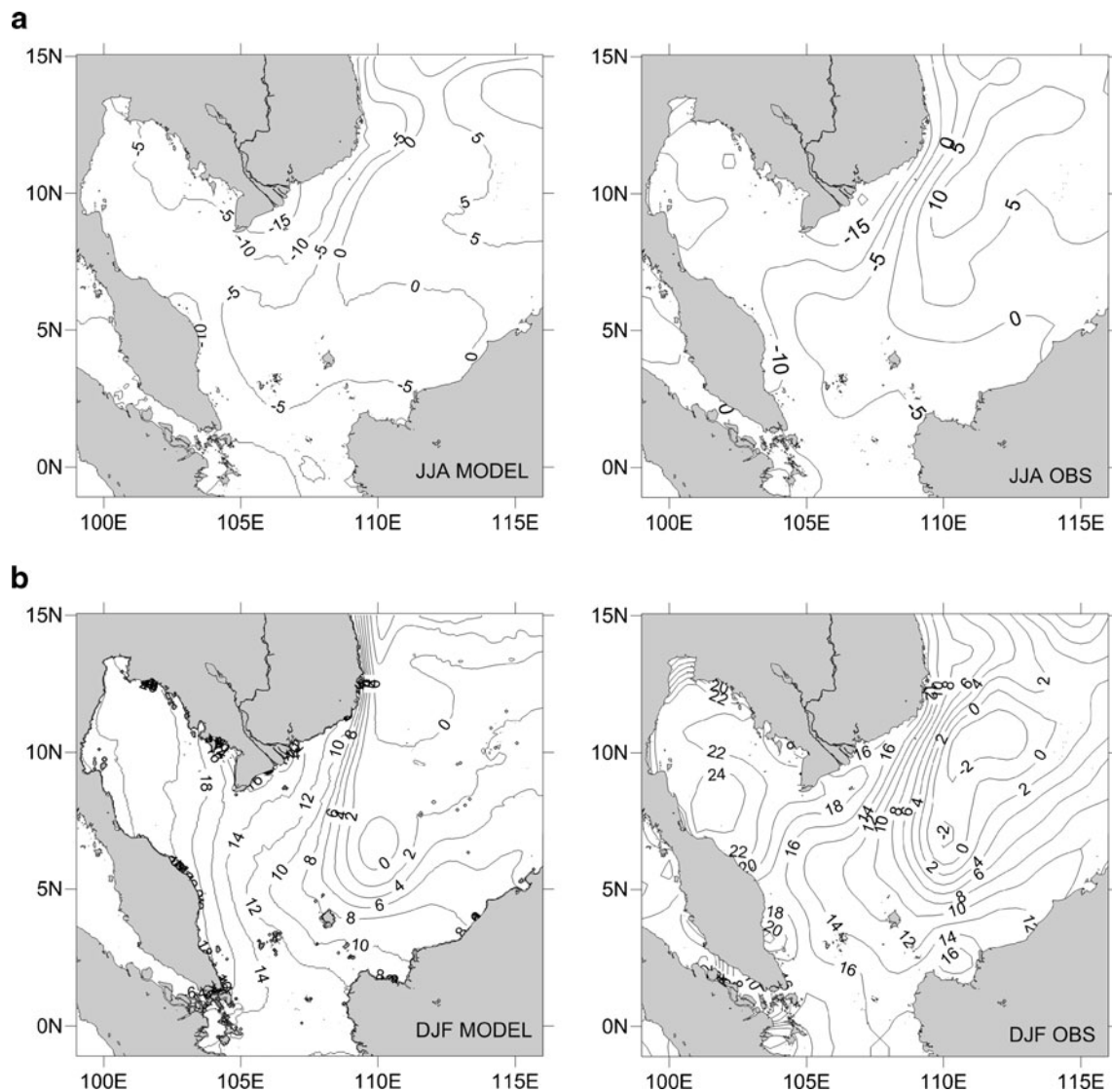

Fig. 7 **a** Modeled (*left*) and observed (*right*, TOPEX/Poseidon) surface elevation anomaly for JJA (units: cm). **b** Modeled (*left*) and observed (*right*, TOPEX/Poseidon) surface elevation anomaly for DJF (units: cm)

(2004) indicated that mixing induced by surface waves played an important role in the formation of upper-ocean mixed layer in spring and summer. More recently, the wave–tide–circulation model has been used successfully to simulate the three-dimensional structure of summertime circulation in the Yellow Sea (Xia et al. 2006) and also the upwelling of Yangtze River Estuary in summer (Lu et al. 2006).

2.2 Model configuration

The model domain encompasses the southern part of the SCS from 3°S–15°N, 99°E–116°E (Fig. 1). The model topography is based on the GEBCO_08 topography data (Downloaded from http://www.gebco.net/). The topography in the model grid is obtained by averaging depth of the nearest 10 grid points in the GEBCO_08. The model resolution is 1/18°×1/18° (6 km), with 51 sigma levels in the vertical. It is forced, unless stated otherwise, by the climatological winds along with surface heat fluxes; tides and open boundary conditions are incorporated. However, both river outflow and evaporative flux are excluded. Both the monthly climatology wind stress and net heat fluxes are

taken from the Comprehensive Ocean-Atmosphere Data Set (COADS; da Silva et al. 1994). The heat flux is applied following Haney (1971):

$$Q = Q_c + \left(\frac{dQ}{dT}\right)_c (T_c^o - T^o)$$

where subscript c represents data from the COADS, Q_c is the net heat flux, dQ/dT is the gradient of the net heat flux with respect to SST, T_c^o is the monthly mean climatological SST from the COADS, and T^o is model SST.

The temperature and salinity fields are initialized, unless stated otherwise, from the Levitus annual mean temperature and salinity (Levitus 1982). The open lateral boundary conditions (velocity, sea level, temperature, and salinity) are interpolated from the output of an Indo-Pacific model of 1/6°×1/6° resolution. The Indo-Pacific model is also the MASNUM wave–tide–circulation coupled model. Its domain is 20°S–50°N, 30°E–150°E. It has the same setup and use the same forcing with the 1/18° model used in this study. Although tides are considered high frequency and commonly ignored in climatological models (e.g., Chu et al. 1999), tidal
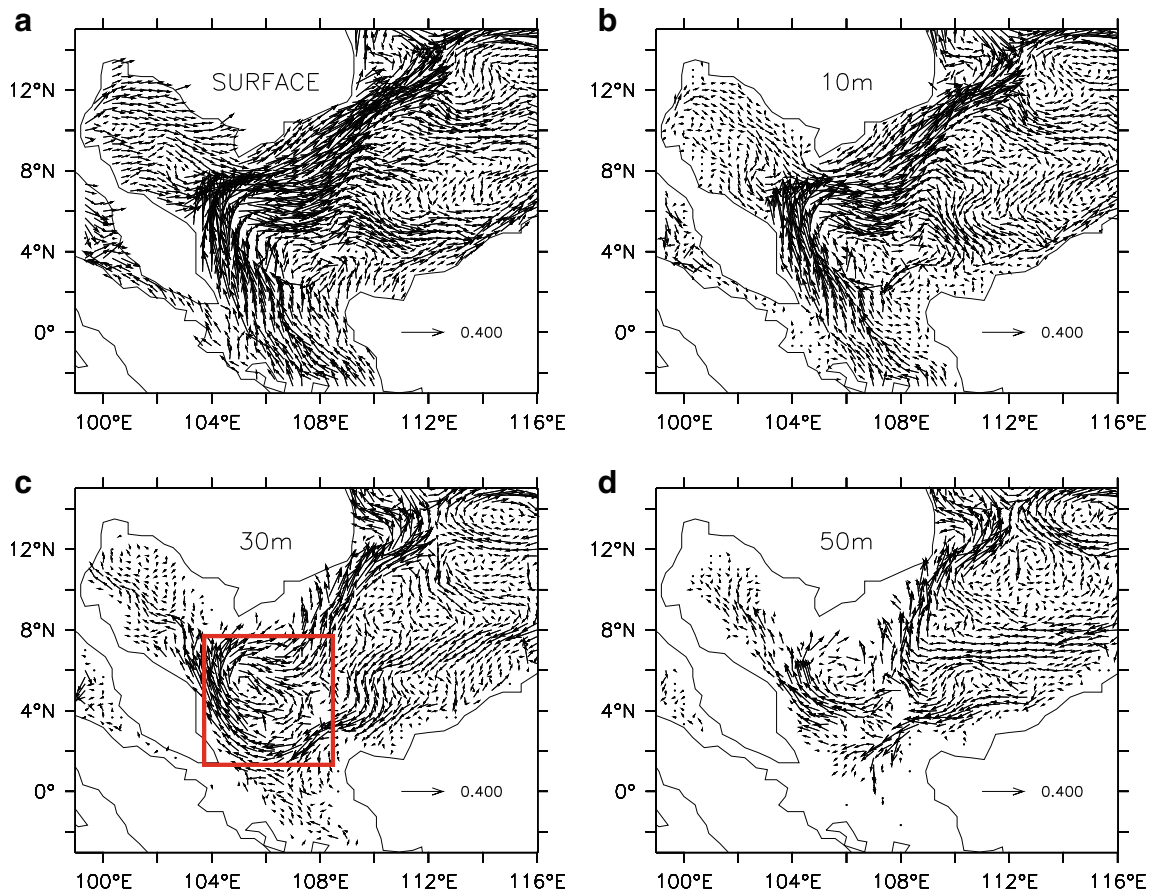

Fig. 8 Flow during JJA at **a** surface, **b** 10 m, **c** 30 m, and **d** 50 m

rectification and tidal-induced mixing are considered in this model by adding the tidal cycle current at the boundary. Tides are considered by adding the tidal current as a radiation condition for the open boundary, that is,

$$U = U_g - (\pm)\sqrt{\frac{g}{H}}(\varsigma_g + \varsigma_T - \varsigma_M)$$

where U_g and ς_g are obtained from the results of the Indo-Pacific model simulation, $(\pm)$ depends on the direction of the outward normal at the open boundary, H and g are water depth and gravitational acceleration, and ς_M is the model computed elevation. ς_T is the tidal elevation,

$$\varsigma_T = A\cos(\omega t - \phi)$$

where ω is the angular frequency, A is the tidal amplitude, and ϕ is the phase lag. The tidal amplitude and lag are obtained from the global $0.25° \times 0.25°$ TPXO.6 tide model of the Oregon State University (Egbert et al. 1994). Four components of tide including M_2, S_2, K_1, and O_1 are considered. To accommodate for the spin-up time, the model is integrated for 20 years, and the simulated fields of the final year are analyzed and presented in this paper.

3 Model validation

3.1 Verification of simulated tide

The model is first run with only tidal forcing and homogenous water by setting temperature and salinity at 15°C and 35 psu in the whole domain, respectively. Figures 3 and 4 show the co-tidal and co-amplitude lines for M_2 and K_1 tide components, respectively. The simulated co-tidal and co-amplitudes lines agree very well with the previous studies (e.g., Fang et al. 1999; Zu et al. 2008). The harmonic constants of M_2 and K_1 tides are plotted in Fig. 5a, b, with values of observed tides of several stations whose locations are indicated as black dots in Fig. 3. For M_2, the mean absolute error of the amplitude is 0.06 m, while the phase is 9.9°. For K_1, the mean absolute error of the amplitude is 0.03 m, while the phase is 7.8°. The observed tidal harmonic constants are from British Admiralty Tide and Tidal Stream Tables.

3.2 Verification of SST

The model simulated seasonal-mean SSTs (left panel) are compared with the observed high-resolution SST climatology (right panel) in Fig. 6a, b. The observed data are from
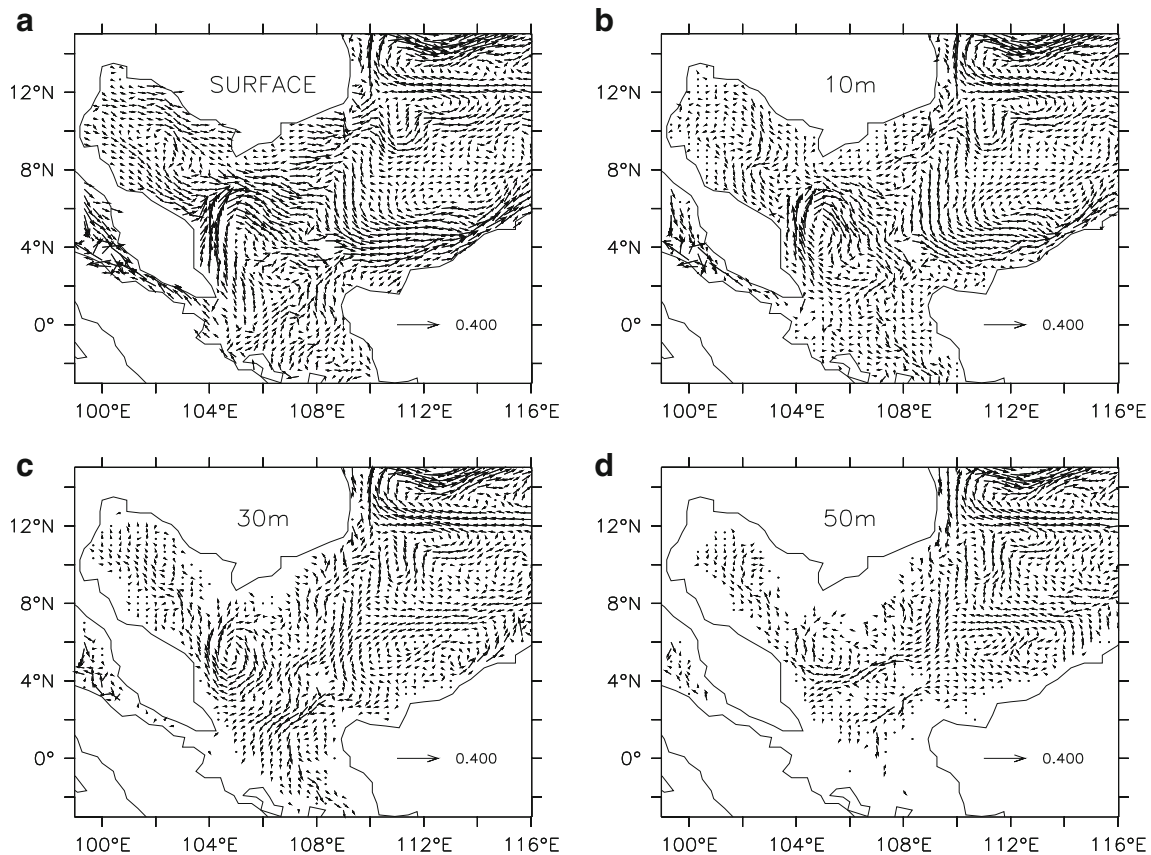

Fig. 9 Same as Fig. 8, except for SON

Reynolds and Smith (1994) with horizontal resolution of 0.088°. During summer, the most important feature of SST is the cold tongue along the Vietnam coast associated with the eastward advection by the SE Vietnam Offshore current. Both the observation and the model show this feature.

During winter (Fig. 6b), the modeled SST pattern also agrees the observation well. There is a temperature front off the Vietnam's southeast coast, which extends to the MPECS. The front is associated with the strong southward current along the west boundary, which brings the cold water from the north to the south.

3.3 Verification of sea surface height

The comparisons between simulated sea surface height (SSH) anomaly and observed SSH anomaly from the TOPEX/Poseidon altimeter data are given in Fig. 7a, b. It can be seen that simulated SSH anomaly pattern broadly agrees with the observation. During summer (Fig. 7a), the SSH anomalies are low over the Sunda Shelf, Gulf of Thailand, and Vietnam coast, while they are high in the northeast part of the region. The SSH anomaly pattern shows that the upper layer circulation of the southern SCS

is dominated by an anti-cyclonic gyre in summer. During winter, the SSH anomalies are high in the Sunda Shelf, Gulf of Thailand, Vietnam coast while low in the northeast part of the region, there exists a low center at (111E,6 N). The SSH anomaly pattern shows that the upper-layer circulation of the southern SCS is dominated by a cyclonic gyre in winter. All the above comparisons show that the model reasonably reproduces the circulation in the region.

4 The simulated circulation results

The simulated seasonally averaged upper-ocean current fields (surface, 10, 30, and 50 m) are given in Figs. 8, 9, 10, 11. In general, the currents are fairly well simulated when compared to observational studies (Dale 1956; Wyrtki 1961; Fang et al. 1998, 2002) and other numerical results (Chu et al. 1999; Yang et al. 2002). Some small-scale circulation patterns can be identified from our model results due to the fine horizontal resolution (~6 km). The circulation in the southern SCS is mainly controlled by the monsoon winds, while here are two transitions in spring
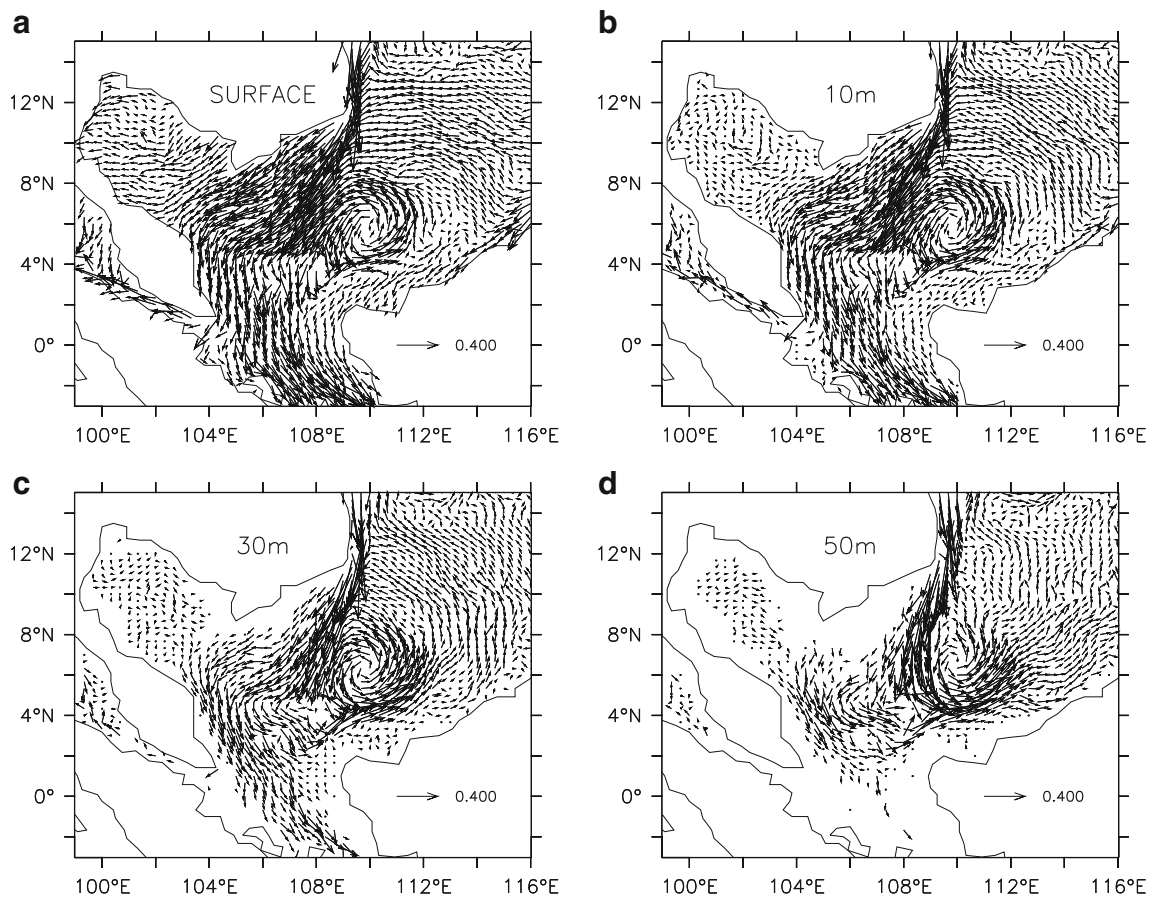

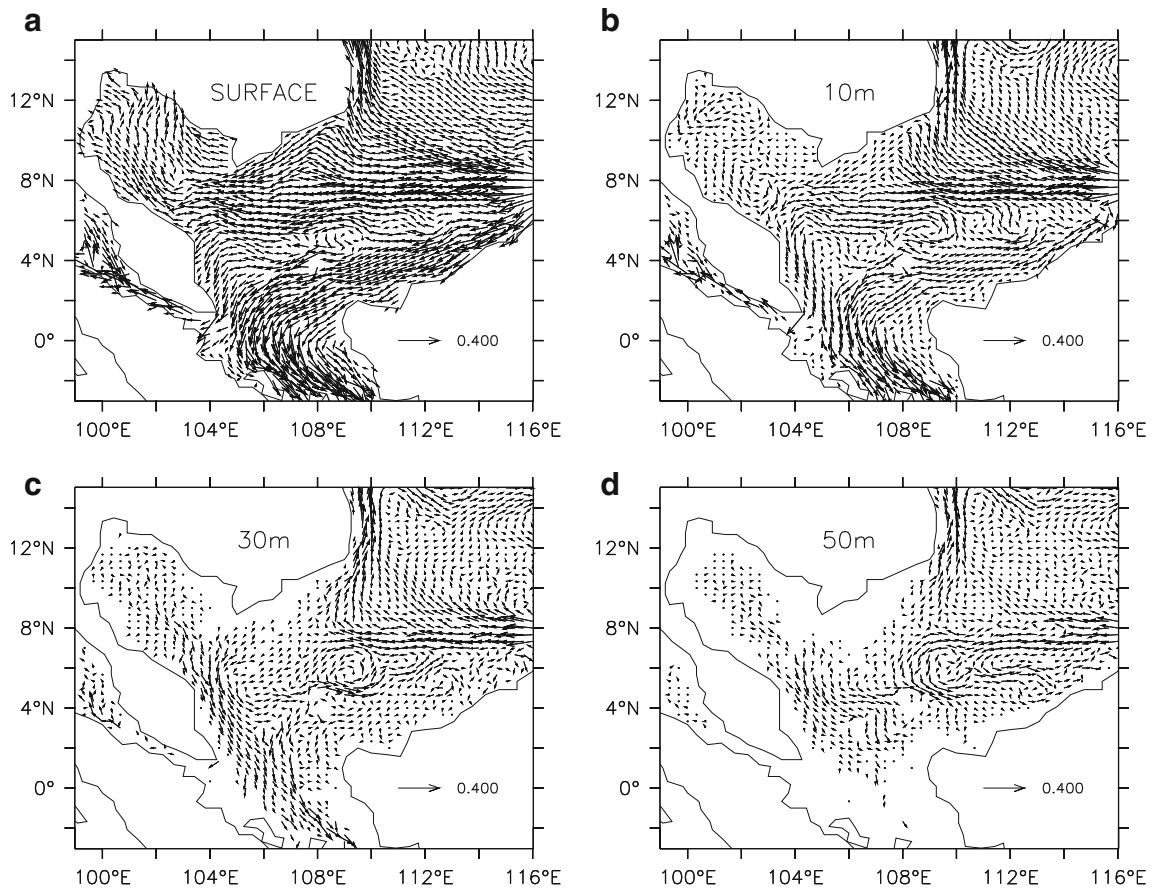
Fig. 10 Same as Fig. 8, except for DJF

Fig. 11 Same as Fig. 8, except for MAM

and fall. The main circulation features are the SCS anti-cyclonic gyre (Fig. 8b, c) during summer and the SCS Southern Cyclonic Gyre (Fig. 10) during winter. In the following sections, we discuss the seasonal circulation patterns with focus on summer and winter.

4.1 Upper-ocean current in summer

The simulated upper-ocean current in summer is given in Fig. 8. In the surface layer (Fig. 8a), the northward flows from the Karimata Strait branch out into a strong western
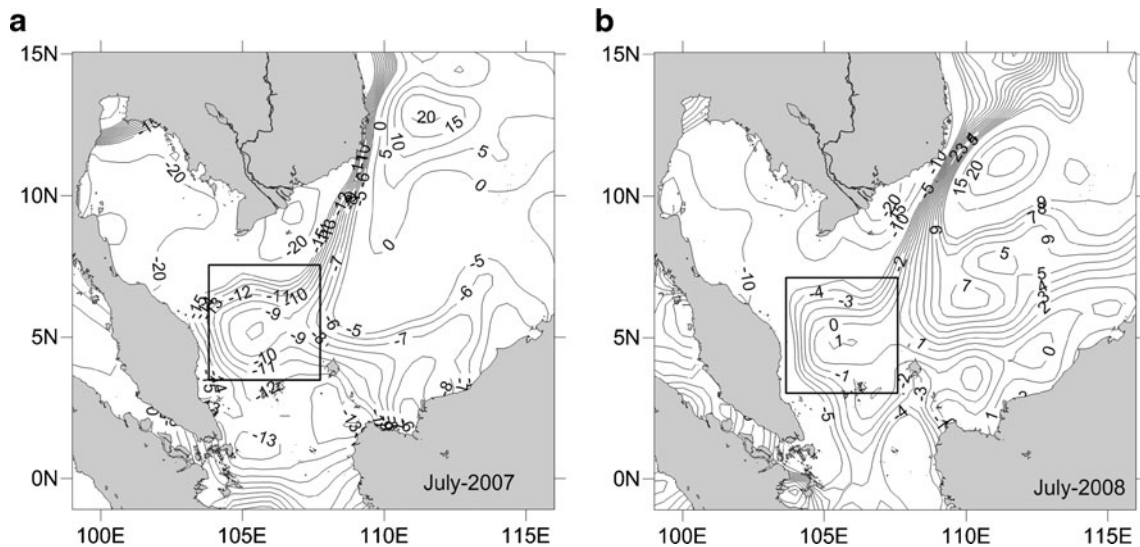

Fig. 12 Monthly mean sea level anomalies from TOPEX/Poseidon altimetry data. a July-2007, b July-2008

boundary that flows along the east coast of Peninsular Malaysia and a weaker component that feeds into the Borneo Coastal Current. In the vicinity of the Natuna Island, a rather weak anti-cyclonic eddy is also simulated, which is consistent with Dale (1956). The northward flowing western boundary current along the east Peninsular Malaysia coast turns northeastward at about 7°N and continues flowing along the Vietnam coast. It turns northeastward and leaves the Vietnam coast between 10°N and 13°N, known as the southeast Vietnam offshore current (SEVOC; Fang et al. 1998).

The current field at the depth of 10 m (Fig. 8b) agrees with the ADCP observations (Fang et al. 2002; Fig. 6a). At this depth, the strong western boundary current and the SEVOC are similar to those in the surface layer. The SEVOC turns southeastward at (112°E, 10°N) and forms the north and east branches of the SCS Southern Anti-cyclonic Gyre (SAG; Fang et al. 1998).

The current field at the depth of 30 m (Fig. 8c) shows the basin-scale SCS SAG more clearly than that at the depth of 10 m. Within the basin-scale anti-cyclonic gyre, an anti-

cyclonic eddy is featured off the Peninsular Malaysia's coast centered at 5°N and 105.5°E with a diameter of about 300–400 km (see the area within the red rectangle in Fig. 8c). In our knowledge, such an eddy has not been highlighted in previous modeling studies or reported by any previous survey. This eddy can be confirmed by the monthly mean TOPEX/Poseidon SSH anomalies in July 2007 and July 2008 (Fig. 12). The observed SSH anomalies show there exists a high center (an anti-cyclonic eddy) off the Peninsular Malaysia's coast centered at 5°N and 105.5°E in July 2007 and July 2008 (see the areas within the rectangles in Fig. 12). The diameter of the eddy is about 300–400 km. Both the center position and the scale of the model reproduced eddy coincide with the observed eddies. The forming mechanism of the eddy will be explored in 4.4 using numerical experiments.

4.2 Upper-ocean current in winter

The simulated upper-ocean current patterns in winter (Fig. 10) are consistent with the previous observations (Dale 1956) and
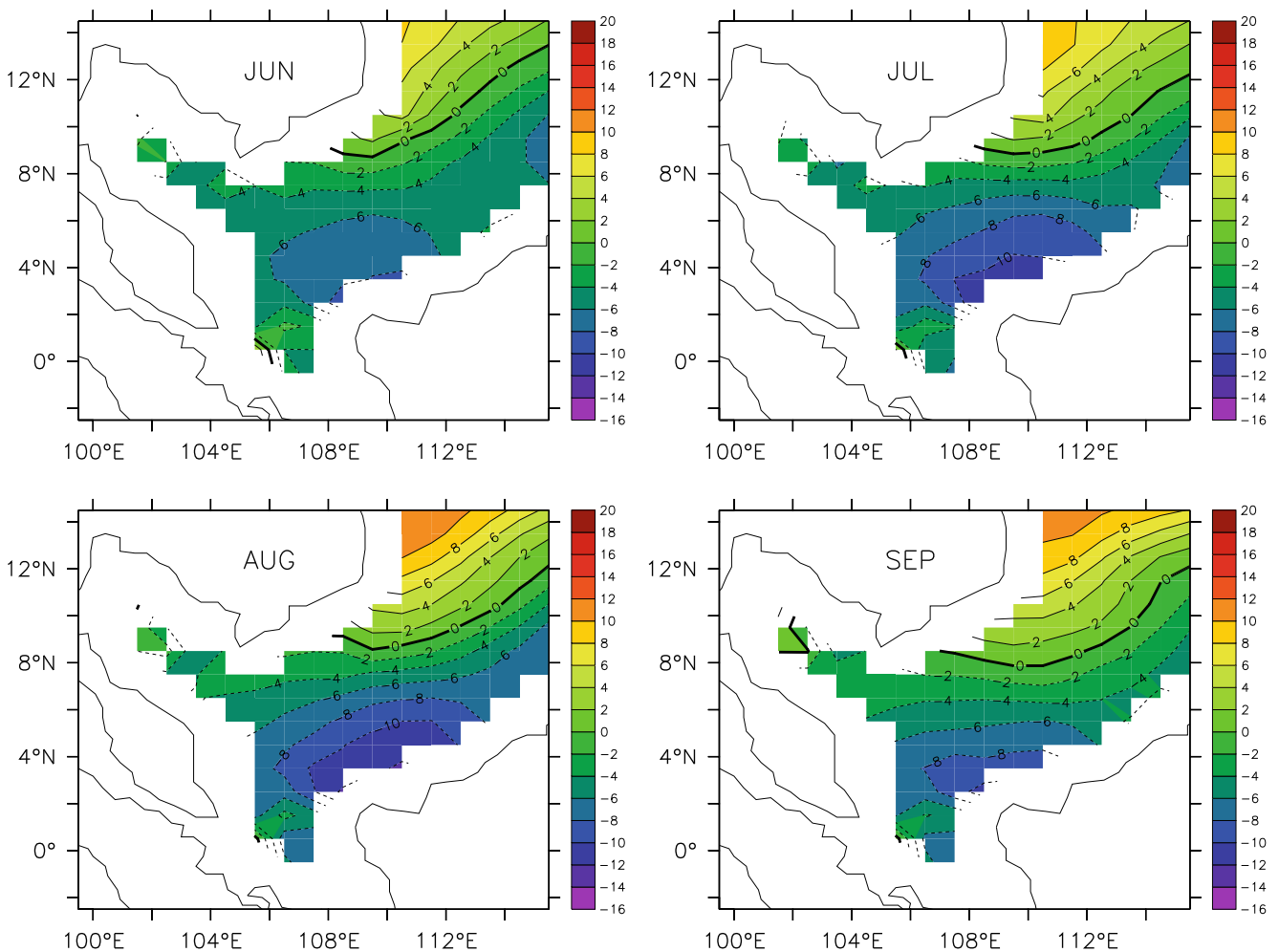

Fig. 13 Monthly mean wind stress curl in June, July, August, and September from COADS dataset (units: 1.0e-8 N/m³)

model results (Chu et al. 1999). The whole southern basin of the SCS experiences a cyclonic circulation. The central westward cross-basin flows feed into the strong and narrow Vietnam coast current that flows southward. Most of the currents flow southward along east coast of the Peninsular Malaysia to the Karimata Strait. A strong cyclonic eddy is also simulated north of the Natuna Island with its center located at 6°N and 110°E. At the eastern side, a much weaker southwestern Borneo Coastal Current is also simulated.

4.3 Upper-ocean current during the monsoon transitions

The circulation patterns during SON (Fig. 9) resemble those during JJA, but are much weaker due to weaker winds in the period. However, the sub-surface cyclonic eddy off the northern Peninsular Malaysia's coast is still present in the simulation. The circulation during MAM (Fig. 11) is somewhat different with the flow in the southern SCS being predominantly a westward cross-basin flow. Stronger and broader Borneo Coastal Currents are simulated, which later feed into the southward flowing western boundary current along the Peninsular Malaysia coast. The northern branch of the cross-basin flow also feeds into northward flowing boundary current along the Vietnam coast.

4.4 The formation mechanism of the eddy off the Peninsular Malaysia's coast in summer

Both wind stress curl and bathymetry steering may be responsible for the formation of the anti-cyclonic eddy off the Peninsular Malaysia's coast centered at (105.5° E, 5°N) in summer (see Section 4.1). The wind stress curls in June, July, August, and September in the region are shown in Fig. 13. They are negative off the Peninsular Malaysia's coast and in the area to the south of 10°N in the region, so the wind is favorable for an anti-cyclonic eddy. The bathymetry in the east Malay Peninsula shelf (Fig. 1, see the area within the red rectangle) shows there exists a basin centered near (105.5°E, 5°N); this kind of bathymetry steering is also favorable for an anti-cyclonic eddy. To reveal the possible mechanism, we designed two more numerical experiments. For Exp 1, the wind stress is set to the domain-averaged wind stress, that is, the wind curl=0. For Exp 2, the model topography shallower than 100 m is set to 100 m except for the region near the open boundary (see the small figure in Fig. 1). Flow fields at the depth of 30 m during the summer in different numerical experiments are shown in Fig. 14. One can see
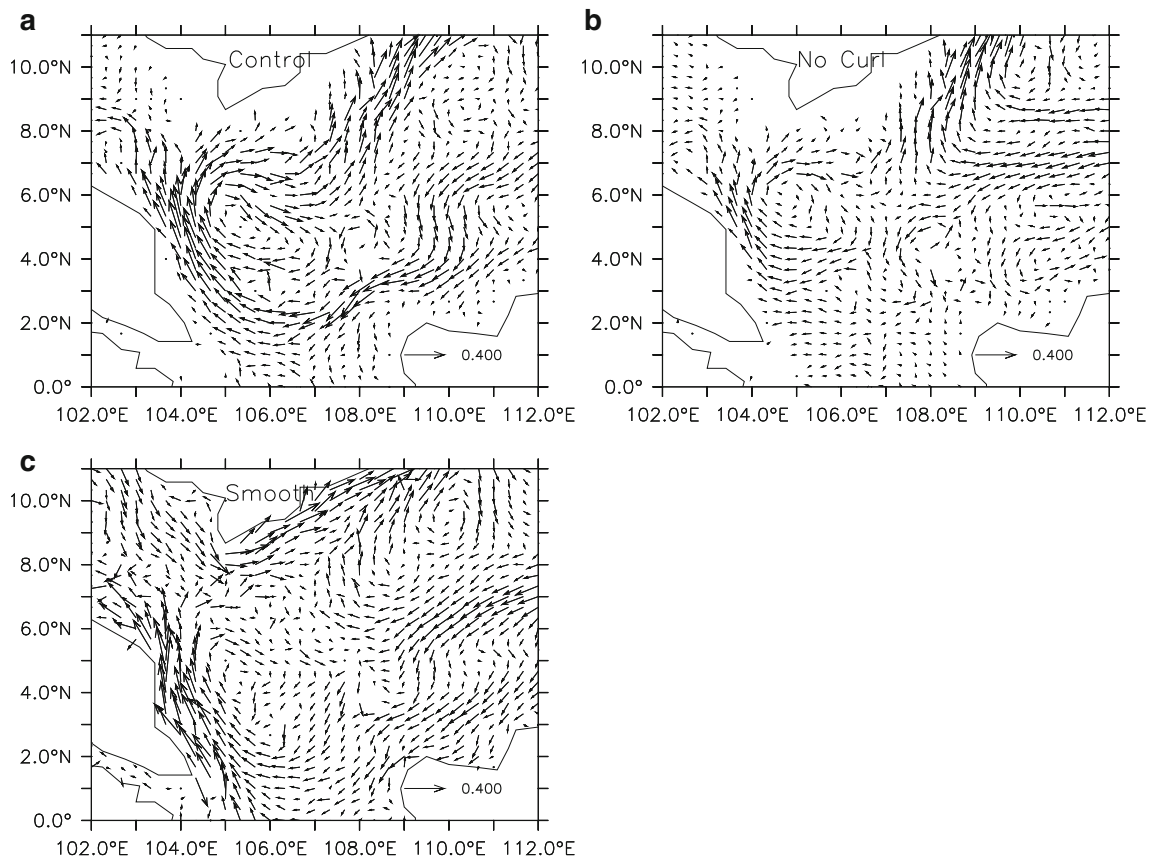

Fig. 14 Flow at the depth of 30 m during JJA in different numerical experiments. **a** Control run, **b** Case with wind curl=0, **c** Case with flat bottom

when the wind curl is set to 0 (Exp 1), the eddy is much weaker and its center changes (Fig. 14b); so the wind stress curl is partly responsible for the formation of the eddy. The basin-scale anti-cyclonic gyre in the southern SCS is also weaker than that in the control run. For the experiment with flat bottom (Exp. 2), the eddy is also weaker especially in the northern part of the eddy (Fig. 14c), without the bathymetry steering the strong flow moving closer to the coast. Exp 2 shows the bathymetry steering is partly responsible for the formation of the eddy. The results of the experiments show that both wind stress curl and bathymetry steering are responsible for the formation of the anti-cyclonic eddy.

5 Conclusions and discussions

The seasonal circulation in MPECS region is studied using a wave–tide–circulation coupled model based on POM. The simulated tidal harmonic constants and temperature structure agree with the observations well. The simulated seasonal circulation patterns also agree with observations. The main currents in the region are well reproduced. The model results show that the upper layer flow field in this region is controlled by the north-east monsoon in winter and south-west monsoon in summer.

An anti-cyclonic eddy is featured off-Peninsular Malaysia's coast centered at 5°N and 105.5°E, the eddy is confirmed by the observed TOPEX/Poseidon sea surface height abnormally. Using two numerical experiments, we find that both wind stress curl and bathymetry steering are responsible for the formation of the anti-cyclonic eddy.

The model successfully reconstructs the seasonal variation of the circulation in the Malay Peninsula East Shelf. Further study is needed to explore the inter-annual variation of the circulation in the region.

References

Chu PC et al (1999) Dynamical mechanisms for the South China Sea seasonal circulation and thermohaline variablities. J Phys Oceanogr 29:2971–2989

da Silva A, Young C, Levitus S (1994) Atlas of Surface Marine Data 1994, vol. 1, Algorithms and Procedures, NOAA Atlas NESDIS 6, U.S. Dep. of Comm., Washington, D. C.

Dale WL (1956) Wind and drift currents in the South China Sea. Malay J tropical Geogr 8:1–31

Egbert GD, Bennett AF, Foreman MGG (1994) TOPEX/POSEIDON tides estimated using a global inverse model. J Geophys Res 99:24821–24852

Fang G et al (1998) A survey of studies on the South China Sea upper ocean circulation. Acta Ocenographica Taiwan 37:1–6

Fang G et al (1999) Numerical simulation of principal tidal constituents in the South China Sea, Gulf of Tonkin and gulf of Thailand. Cont Shelf Res 19:845–869

Fang G et al (2010) Volume, heat and freshwater transports from the South China Sea to Indonesian Seas in the boreal winter of 2007–2008. J Geophys Res 115:C12020

Fang W et al (2002) Seasonal structures of upper layer circulation in the southern South China Sea from in situ observations. J Geophys Res 107(C11):3202. doi:10.1029/2002JC001343

Haney R (1971) Surface thermal boundary condition for ocean circulation models. J Phys Oceanogr 1:241–248

Hu J et al (2000) A review on the currents in the South China Sea: seasonal circulation, South China Sea warm current and Kuroshio intrusion. J Oceanogr 56:607–624

Levitus S (1982) Climatological Atlas of the World Ocean. NOAA Prof. Paper No. 13, U. S. Govt. Printing Office, 173 pp. plus 17 microfiche

Li L, Wu R, Guo X (2000) Seasonal circulation in the South China Sea:A TOPEX/Poseidon satellite altimetry study. Acta Oceanologica Sinica 22:11–26

Lu X, Qiao F, Xia C, Zhu J, Yuan Y (2006) Upwelling off Yangtze River estuary in summer. J Geophys Res 111:C11S08. doi:10.1029/2005JC003250

Mellor GL, Yamada T (1982) Development of a turbulence closure model for geophysical fluid problems. Rev Geophys Space Phys 20:851875

Qiao F, Yuan Y, Yang Y, Zheng Q, Xia C, Ma J (2004) Wave induced mixing in the upper ocean: Distribution and application to a global ocean circulation model. Geophys Res Lett 31:L11303. doi:10.1029/2004GL019824

Reynolds RW, Smith TM (1994) Improved global sea surface temperature analyses using optimum interpolation. J Climate 7:929–948

Shaw PT, Chao SY (1994) Surface circulation in the South China Sea. Deep Sea Res I 41:1663–1683

Wang D, Liu Y, Qi Y, Shi P (2001) Seasonal variability of thermal fronts in the northern South China Sea from satellite data. Geophys Res Lett 28:3963–3966

Wyrtki K (1961) Scientific results of marine investigations of the South China Sea and the Gulf of Thailand 1951–1961. Naga report, Vol. 2, University of California at San Diego, 164–169

Xia C et al (2006) Three-dimensional structure of the summertime circulation in the Yellow Sea from a wave–tide–circulation coupled model. J Geophys Res 111:C11S03. doi:10.1029/2005JC003218

Yang H et al (2002) A general circulation model study of the dynamics of the upper ocean circulation of the South China Sea. J Geophys Res 107(7):3085. doi:10.1029/2001JC001084

Zu T, Gan J, Erofeevac SY (2008) Numerical study of the tide and tidal dynamics in the South China Sea. Deep Sea Res I 55:137–154